

Y.-Y. Lin · S.-P. Lo

A study of a finite element model for the chemical mechanical polishing process

Received: 15 April 2002 / Accepted: 28 June 2002 / Published online: 27 March 2004
© Springer-Verlag London Limited 2004

Abstract In this paper, relative velocity at a given point on the wafer was first derived. The revolutions of wafer and pad are assumed the same and the axisymmetric uniformly distributed pressure form is given. Thus, a 2D axisymmetric quasic-static model for chemical-mechanical polishing process (CMP) was established. Based on the principle of minimum total potential energy and axisymmetric elastic stress-strain relations, a 2D axisymmetric quasic-static finite element model for CMP was thus established. In this model, the four-layer structures including wafer carrier, carrier film, wafer and pad are involved. The von Mises stress distributions on the wafer surface were analysed, the effects of axial, hoop, radial and shear stresses to von Mises stress and the effects of axial, hoop, radial and shear strains to deformation of the wafer were investigated. The findings indicate that near the wafer centre, von Mises stress distribution on the wafer surface was almost uniform, then increased gradually with a small amount. However, near the wafer edge, it would decrease in a large range. Finally, it would increase dramatically and peak significantly at the edge. Besides, the axial stress and strain are the dominant factors to the von Mises stress distributions on the wafer surface and the wafer deformation, respectively.

Keywords CMP · Wafer carrier · Carrier film · Wafer · Pad · 2D axisymmetric quasi-static model · Finite element model

1 Introduction

Chemical mechanical polishing process, or CMP for short, is mainly to utilise the pressure applied on the top surface of the wafer carrier, polishing of the pad and injection of the slurry to polish and remove the metallic film on the wafer surface to attain the required planarisation. For the future semiconductor industry, due to the enhancement of precision and capabilities of electronic devices and the increase in storage space and memory capacity, it is inevitable that the size of wafer must be enlarged. Besides, the demand of lithographic exposure resolution increases relatively when the size of component decreases progressively because that the optical system resolution capacity of stepper must be strengthened by short-wavelength ultraviolet. It induces that the smaller the depth of focus of optical development is, the more strict the demand of nonuniformity of the wafer surface is. Therefore, the global planarisation technology becomes increasingly important and CMP is the most important method in this field.

Figure 1 shows the illustration of CMP. It consists of wafer carrier, carrier film, pad and platen. The carrier is attached to the wafer back by means of vacuum. The wafer surface, i.e. the IC part to be planarised, is placed on the platen with one or more layers of pads. Slurry is sprayed continuously through a tube and uniformly scattered on the pad. The wafer is placed between the carrier and pad. The relative motion generated by the carrier and platen brings the wafer in contact with particles in the slurry, which generates the multiple actions including the mechanical friction, chemical reaction and removal of chemical solvent to accomplish the highly efficient material removal.

It is known from Fig. 1 that the CMP mechanism is very complicated intrinsically to not understand very clearly yet. It is extremely difficult to analyse its polishing mechanism. Therefore, it is necessary to simplify the CMP model. Runnels and Renteln [1] used an axisymmetric model under the three assumptions including no

Y.-Y. Lin (✉) · S.-P. Lo
Department of Mechanical Engineering,
De Lin Institute of Technology, 1, 380 LN,
Chin-Yung Road, Tucheng, Taipei Hsien, Taiwan ROC
E-mail: loulin@ms17.hinet.net

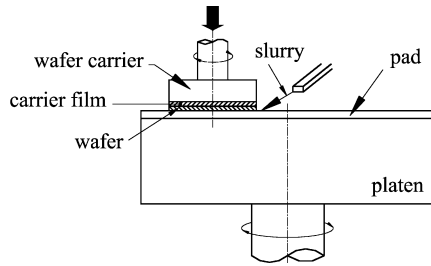


Fig. 1 Illustration of CMP

force transmission between the pad and wafer; an elastic pad and ignoring the effect of slurry, to simulate the stress distribution on the wafer surface and rewrite the Preston's equation to infer the correlation between the stress and material removal rate. The result indicated that the normal stress had a significant effect on the removal rate. Runnels and Eyman [2] applied fluid dynamics to describe the action of chemical solvent. The model is satisfied simultaneously with the slurry transport model and physical erosion model, but the latter is much closer to the experimental result. Kaanta and Landis [3] designed a wafer carrier composed of two different materials. The result showed that the upward deflection of the carrier caused by the difference of expansion coefficients compensates the polishing effect produced by nonuniform distribution of the abrasives, but it seems not easy to control the deflection of carrier precisely. Wang et al. [4] established a 2D axisymmetric elastic model for CMP. The effect of slurry is ignored and the shear stress of the wafer surface assumes to be uniformly distributed on the surface. The von Mises stress distribution on the wafer surface is used to explore the wafer nonuniformity. The simulation results using the commercial software package I-DEAS confirmed that the von Mises stress distribution did have an effect on the surface nonuniformity. Srinivasa-Murthy et al. [5] established a 3D elastic model to study the variation of the wafer surface when sustaining force during the CMP process. The result simulated by the commercial software package ANSYS showed that the peak of the von Mises stress distribution occurs at the edge. The profile of the stress distribution is similar to that in [4], but the site of stress peak is somewhat different. Baker [6] derived the deformation between the wafer and pad, and the stress distribution while regarding the pad as an elastic plane. Yu [7] used the Hertzian contact theory to explain the correlation between the deformation on the contact interfaces and the removal rate. Tseng [8] used a thin plate as a wafer to calculate the stress distribution between the wafer and pad by means of the strain energy and the Hertzian contact theory. Castillo-Mejia et al. [9] described a 2D finite element wafer scale model for chemical mechanical polishing using the commercial software package ANSYS. The result showed good qualitative agreement between observed CMP nonuniformities obtained on Applied Materials' Mirra polisher and the distribution of calculated von Mises stresses on

the wafer surface. Ahmadi and Xia [10] used the mechanical contact theory to analyse the abrasive particle-surface interactions and to study the processes of surface removal by adhesive and abrasive wear mechanisms during chemical mechanical polishing and they developed a model for interactions of pad asperities with abrasive particles.

2 Theoretical foundations

2.1 Preston's equation

CMP is used mainly for material removal of the wafer surface. The material removal rate (MRR) during the CMP process can be considered as a function of the applied normal pressure and the relative velocity. It can be expressed by Preston's equation, i.e.

$$MRR = C_p \times P \times V \quad (1)$$

Note that P is the normal pressure, V relative velocity and C_p the Preston's constant.

2.2 Relative velocity of point A on the wafer

In Eq. 1, the normal pressure can be controlled during the polishing process. The relative velocity can be deduced into the relation between revolutions of the wafer and pad. Figure 2 illustrates the relative motion between the wafer and pad. For point A on the wafer, its relative velocity to the pad can be expressed as:

$$\vec{V} = \vec{V}_w - \vec{V}_p \quad (2)$$

Note that \vec{V} is the relative velocity of point A on the wafer to the pad, \vec{V}_w the absolute velocity of point A on the wafer and \vec{V}_p the absolute velocity of point A on the pad.

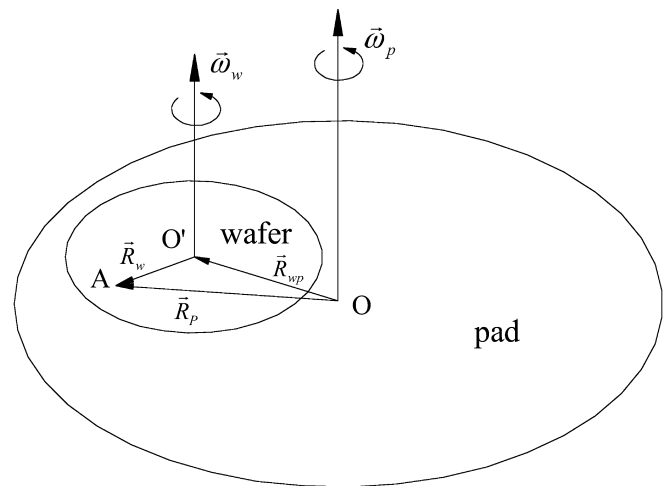


Fig. 2 Illustration of the relative motion between the wafer and the pad

In Eq. 2:

$$\vec{V}_w = \vec{R}_w \times \vec{\omega}_w$$

$$\vec{V}_p = \vec{R}_p \times \vec{\omega}_p \quad (3)$$

Note that \vec{R}_w is the distance from point A to the wafer centre, O' ; $\vec{\omega}_w$ is revolution of the wafer, \vec{R}_p the distance from point A to the pad centre, O ; $\vec{\omega}_p$ revolution of the pad.

Incorporate Eq. 3 into Eq. 2, then

$$\begin{aligned} \vec{V} &= \vec{R}_w \times \vec{\omega}_w - \vec{R}_p \times \vec{\omega}_p \\ &= \vec{R}_w \times \vec{\omega}_w - (\vec{R}_w + \vec{R}_{wp}) \times \vec{\omega}_p \\ &= \vec{R}_w \times (\vec{\omega}_w - \vec{\omega}_p) - \vec{R}_{wp} \times \vec{\omega}_p \end{aligned} \quad (4)$$

Note that \vec{R}_{wp} is the distance between the pad centre and wafer centre, OO' .

2.3 2D axisymmetric quasi-static model for CMP

In order to develop the finite element model for CMP, the kinematics model of CMP must be firstly established. It showed in [11] that the pressure generated by the slurry film between the pad and wafer is small compared with the down pressure applied on the carrier. Thus, it can assume that the pressure exerted on the wafer surface comes mainly from the carrier.

Stresses on the wafer surface arise mainly from two sources, namely the pressure exerted by the carrier and the shear stress due to the relative motion between the wafer and pad. Both the wafer and pad assume to have the same revolution, i.e.,

$$\vec{\omega}_w = \vec{\omega}_p \quad (5)$$

The relative velocity of point A on the wafer to pad in Eq. 4 then reduces to:

$$\vec{V} = -\vec{R}_{wp} \times \vec{\omega}_p \quad (6)$$

Obviously, it is a constant value. It results in a constant shear stress that is uniformly distributed on the wafer surface-pad interface. Therefore, the effect of shear stress can be neglected and a quasi-static model is established. Next, the force is axisymmetrically distributed and the axisymmetric geometry of pad can be achieved assuming that it possesses a huge smooth surface. Hence, the model can be simplified into a 2D axisymmetric quasi-static model for CMP as shown in Fig. 3.

2.4 Principle of minimum total potential energy

While an elastic body is exerted by body force and surface force, its total potential energy can be defined as

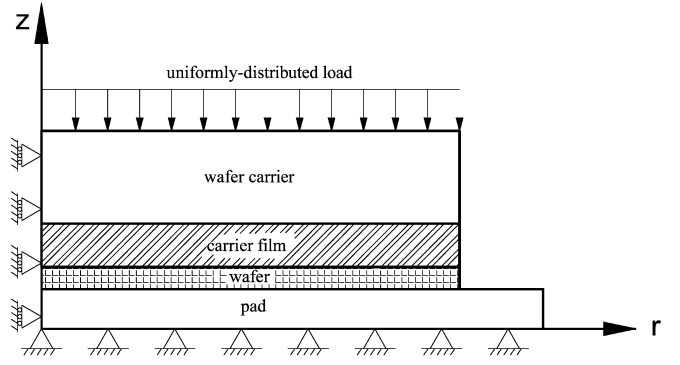


Fig. 3 2D axisymmetric quasi-static model for CMP

$$\Pi = U_P - V_P \quad (7)$$

Note that Π is the total potential energy, U_P the strain energy and V_P the work done on the body by the applied load.

In Eq. 7, the strain energy is defined as

$$U_P = \frac{1}{2} \iiint_V \{\varepsilon\}^T \{\sigma\} dV \quad (8)$$

Note that $\{\varepsilon\}$ is strain row vector, $\{\sigma\}$ stress row vector and V the volume. For a 2D axisymmetric case, $\{\varepsilon\} = \{\varepsilon_{rr} \ \varepsilon_{\theta\theta} \ \varepsilon_{zz} \ \gamma_{rz}\}^T$ and $\{\sigma\} = \{\sigma_{rr} \ \sigma_{\theta\theta} \ \sigma_{zz} \ \tau_{rz}\}^T$.

And, the work done by the applied load can be expressed as

$$V_P = \iiint_V \{d\}^T \{F_b\} dV + \iint_s \{d\}^T \{T_d\} dS \quad (9)$$

Note that d is the displacement, $\{F_b\}$ the body force, $\{T_d\}$ the surface tractions and S the surface of the body on which surface tractions are prescribed.

The principle of minimum potential energy can be described that of all possible displacement states (u and v), it assumes that a body satisfies compatibility and given kinematic or displacement boundary condition, in the mean while, the state which satisfies the equilibrium equations makes the potential energy be a minimum value. [12]

If the potential energy, Π is expressed in terms of the displacements u and v , the principle of minimum potential energy gives, at the equilibrium state,

$$\delta\Pi(u, v) = \delta U_P(u, v) - \delta V_P(u, v) = 0 \quad (10)$$

2.5 2D axisymmetric finite element formulation

Considering a typical 2D triangular element, “e”, shown in Fig. 4, its nodal displacement vector can be expressed as

$$\{\delta\} = \{u_i, v_i, u_j, v_j, u_k, v_k\} \quad (11)$$

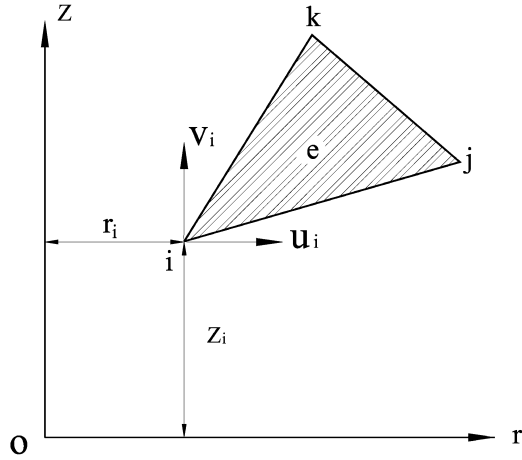


Fig. 4 Typical 2D triangular element, e

Note that δ is the nodal displacement vector, u and v the displacements along r and z directions, respectively.

A displacement function of an arbitrary point in an element is defined as

$$\{d\} = [N]\{\delta\} \quad (12)$$

Note that $\{d\}$ is the displacement function and $[N]$ the shape function matrix.

The 2D strain-displacement relations can be expressed in the form of nodal displacement as

$$\{\varepsilon\} = \begin{Bmatrix} \varepsilon_{rr} \\ \varepsilon_{\theta\theta} \\ \varepsilon_{zz} \\ \gamma_{rz} \end{Bmatrix} = \begin{Bmatrix} \frac{\partial u}{\partial r} \\ \frac{u}{r} \\ \frac{\partial v}{\partial z} \\ \frac{\partial u}{\partial z} + \frac{\partial v}{\partial r} \end{Bmatrix} = [B]\{\delta\} \quad (13)$$

Note that $[B]$ is the strain-displacement matrix.

Introduce the stress-strain relations based on the Hooke's law as expressed in the following

$$\{\sigma\} = [D^e]\{\varepsilon\} \quad (14)$$

Note that $[D^e]$ is the elastic stress-strain relation matrix.

Then, the strain energy becomes as while substituting Eqs. 13 and 14 into Eq. 8

$$U_P(u, v) = \frac{1}{2} \iiint_V \{\delta\}^T [B]^T [D^e] [B] \{\delta\} dV \quad (15)$$

Besides, the work done by the applied load can be given by while incorporating Eq. 12 into Eq. 9

$$V_P(u, v) = \iiint_V \{\delta\}^T [N]^T \{F_b\} dV + \iint_S \{\delta\}^T [N]^T \{T_d\} dS \quad (16)$$

Substituting Eqs. 15 and 16 into Eq. 7, the total potential energy of an elastic body becomes as

$$\begin{aligned} \Pi(u, v) &= \frac{1}{2} \iiint_V \{\delta\}^T [B]^T [D^e] [B] \{\delta\} dV \\ &\quad - \iiint_V \{\delta\}^T [N]^T \{F_b\} dV \\ &\quad - \iint_S \{\delta\}^T [N]^T \{T_d\} dS \end{aligned} \quad (17)$$

Incorporate Eq. 17 into Eq. 10 and take first variation with respect to the displacements, we get

$$\{\Delta\delta\}^T ([K]_e \{\delta\} - \{Q\}_e) = 0 \quad (18)$$

Note that

$$[k]_e = \iiint_V [B]^T [D^e] [B] dV$$

$$\{Q\}_e = \iiint_V [N]^T \{F_b\} dV + \iint_S [N]^T \{T_d\} dS$$

As a result, we obtain

$$[K]_e \{\delta\} = \{Q\}_e \quad (19)$$

Expressing step by step in terms of the whole domain, a 2D elastic finite element governing equation is given by

$$[K]\{\delta\} = \{Q\} \quad (20)$$

Note that $[K]$ is the elastic stiffness matrix, i.e., $[K] = \sum_1^n [K]_e$ and $\{Q\}$ the nodal force, i.e., $\{Q\} = \sum_1^n \{Q\}_e$.

3 A summary of the chemical mechanical polishing process simulation

A 2D axisymmetric quasi-static model for CMP and a theoretical foundation of 2D axisymmetric finite element model have been established. A flowchart of the technique to simulate the CMP process is shown in Fig. 5.

The description of the procedures which were developed to simulate a CMP process is as follows:

1. A 2D axisymmetric quasi-static model for CMP was established in Eq. 6, i.e. $\bar{V} = -\bar{R}_{wp} \times \bar{\omega}_p$.
2. A 2D axisymmetric finite element model for CMP was developed in Eq. 20, i.e., $[K]\{\delta\} = \{Q\}$.
3. Input the boundary conditions and carrier pressure.
4. Solve Eq. 20, i.e., $[K]\{\delta\} = \{Q\}$ to achieve the nodal displacements, $\{d\}$.
5. Solve Eq. 12, i.e., $\{d\} = [N]\{\delta\}$ and Eq. 13, i.e., $\{\varepsilon\} = [B]\{\delta\}$ to obtain the element strain, $\{\varepsilon\}$.
6. Solve Eq. 14, i.e., $\{\sigma\} = [D^e]\{\varepsilon\}$ to obtain the element stress, $\{\sigma\}$.
7. Take the strain, $\{\varepsilon\}$ and stress, $\{\sigma\}$ in the neighbouring of wafer-pad interface to transfer into the nodal strain and stress in the wafer-pad interface.

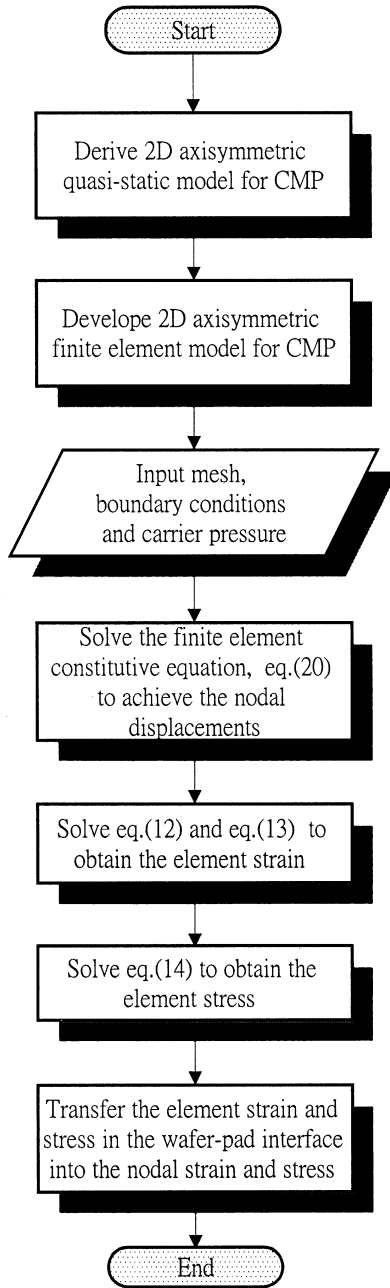


Fig. 5 Flowchart of the CMP process simulation

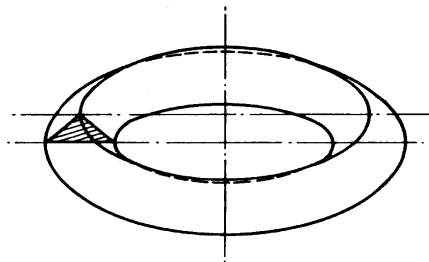


Fig. 6 Typical 2D axisymmetric hoop element [12]

4 Case study

The following basic assumptions are made in this study:

1. The surfaces of the carrier, carrier film, wafer and pad are smooth.
2. Materials including the carrier, carrier film, wafer and pad are all isotropic.
3. All materials are tightly stacked.

Based on the 2D axisymmetrical characteristics in the developed CMP model, it can be stacked up by a “ring” element in which its cross section is a typical triangular element as shown in Fig. 6 [12]. In Fig. 3, there are a total of 6,800 triangular elements and 3,661 nodes in the finite element mesh and the boundary conditions are assumed as follows:

1. Only a uniformly distributed down pressure is considered, and it is applied on the top surface of carrier.
2. The bottom surface of the pad sustains a fixed support, while nodes at the bottom are subject to complete limitation in all directions.
3. The left side is a symmetric boundary condition and enjoys a roller support, while nodes at this side are r direction limitation and able to move freely in z direction.
4. The displacements of adjacent nodes across the carrier-film, film-wafer and wafer-pad interfaces sustain the same amount in all directions.

The down pressure applied on the top surface of the carrier was set at 0.069 MPa. The material properties and geometries are listed in Table 1. [5]

5 Results and discussion

Von Mises proposed in 1913 that yielding occurs when a combination of stresses (i.e., von Mises stress) exceeds the material’s yield strength. The von Mises stress applied in 2D axisymmetric quasi-static CMP model can be simplified as

$$\bar{\sigma} = \frac{1}{\sqrt{2}} \left[(\sigma_{rr} - \sigma_{zz})^2 + (\sigma_{zz} - \sigma_{\theta\theta})^2 + (\sigma_{rr} - \sigma_{\theta\theta})^2 + 6\tau_{rz}^2 \right]^{\frac{1}{2}} \quad (21)$$

Note that $\bar{\sigma}$ is the von Mises stress, σ_{rr} , $\sigma_{\theta\theta}$, σ_{zz} and τ_{rz} the radial, hoop, axial and shear stresses, respectively.

Table 1 Material properties and geometries [5]

	Modulus of elasticity (MPa)	Poisson’s ratio	Radius (mm)	Thickness (mm)
Wafer carrier	193054.4	0.3	100.33	7.62
Carrier film	0.2654	0.1	100.33	0.635
Wafer	193054.4	0.3	100.33	0.706
Pad	2.2891	0.1	558.8	1.397

Under the condition of ignoring the chemical action of slurry, the 0.069 MPa down pressure was applied on the top surface of the carrier and the von Mises stress distributions on the wafer surface were simulated with the developed finite element model. Figure 7a shows the correlation between the calculated von Mises stress distributions and the distance from the wafer centre. To understand much more about the variation of part of lower von Mises stress distributions in Fig. 7a, the wafer

centre stress was regard as a basis. The stress difference has been obtained after comparing it with other node stresses on wafer surface, and the comparison was plotted in Fig. 7b. From Figs. 7a and b, it is shown that near the wafer centre, von Mises stress distribution was almost uniform, then increased gradually with a small amount. However, near the wafer edge, it would decrease in a large range. Finally, it would increase dramatically and peak significantly at the edge. This result was similar to that of [5].

Figure 8 is an experimental removal rate variation diagram by using two different carrier films. The curves in Fig. 8 are oxide-polishing results obtained with two carrier films, R200T3 and DF200, which have moduli of elasticity of 0.69 MPa and 0.407 MPa, respectively. [4] It shows that there is a significant variation in material removal rate from the average values at the edge for two films. While comparing between Figs. 7a, b and Fig. 8. Although the simulated conditions in this paper was a

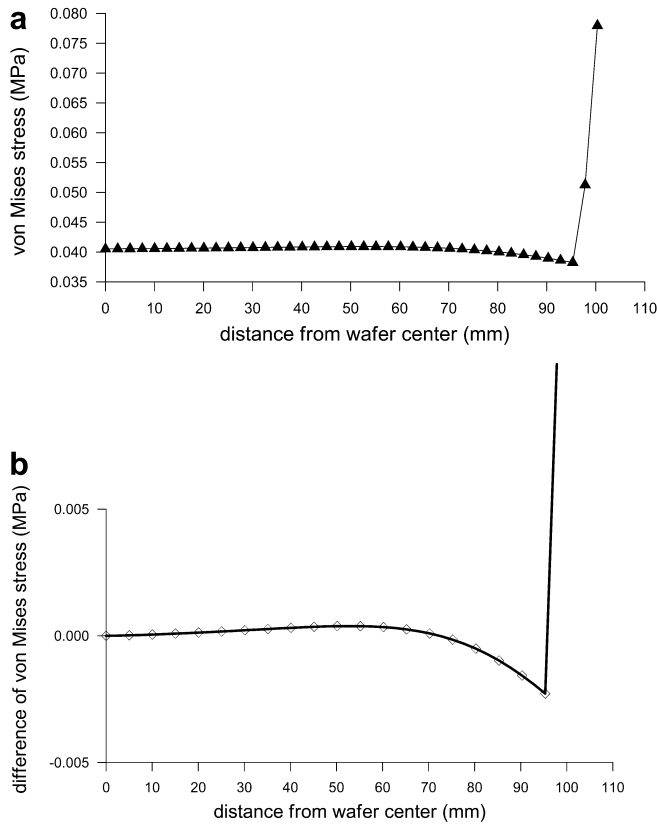


Fig. 7 a Von Mises stress distributions on the wafer surface b Difference of von Mises stress on the wafer surface

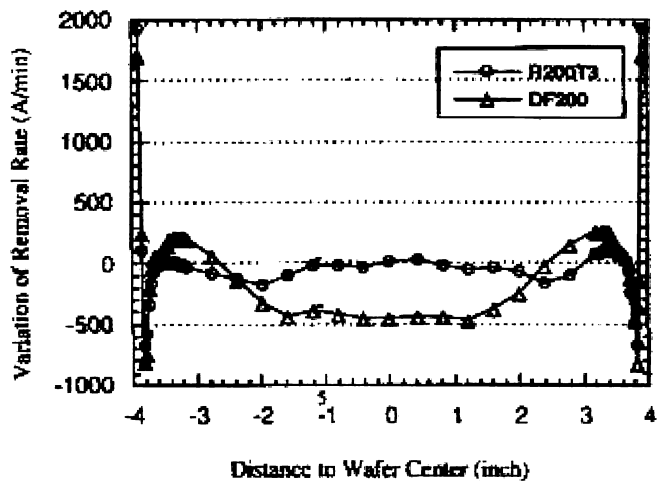


Fig. 8 Experimental material removal rates on wafer surface [4]

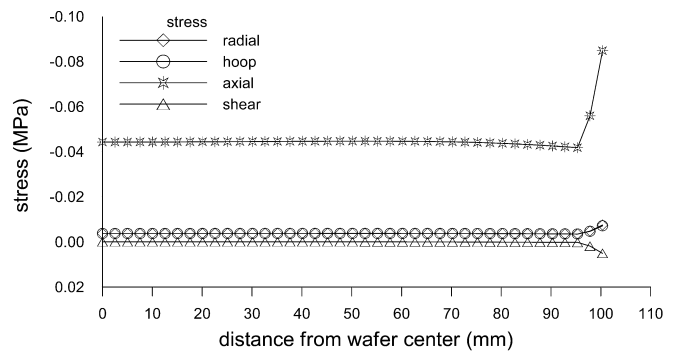


Fig. 9 Axial, hoop, radial and shear stress distributions on the wafer surface

Table 2 Stress components on the wafer centre and the maximum for each stress on the wafer surface

Stress components	On wafer centre	Maximum
σ_{rr} (radial stress)	-0.37093940E-02	-0.74636508E-02
$\sigma_{\theta\theta}$ (hoop stress)	-0.37093608E-02	-0.71316257E-02
σ_{zz} (axial stress)	-0.44246150E-01	-0.84756205E-01
τ_{rz} (shear stress)	-0.36209338E-05	0.50688152E-02

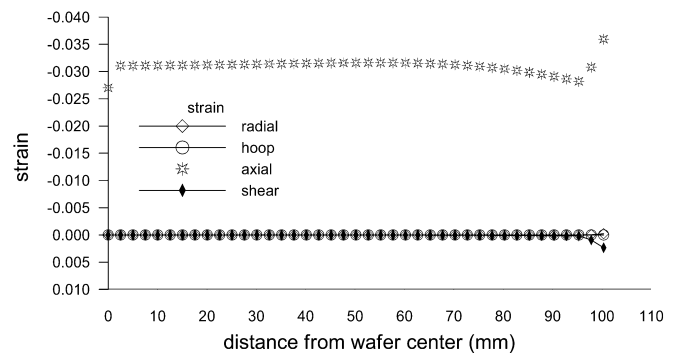


Fig. 10 Axial, hoop, radial and shear strain distributions on the wafer surface

Table 3 Strain components on the wafer centre and maximum for each strain on wafer surface

Strain components	On wafer centre	Maximum
ε_{rr} (radial strain)	-0.65632324E-06	-0.23499126E-03
$\varepsilon_{\theta\theta}$ (hoop strain)	-0.64600783E-06	-0.22162025E-05
ε_{zz} (axial strain)	-0.26993460E-01	-0.35939880E-01
γ_{rz} (shear strain)	-0.36513438E-05	0.23517157E-02

little different from that of the material removal experiment shown in Fig. 8, the profile of the von Mises stress distributions in Figs. 7a and b is also similar to that of the removal rate, i.e., the characteristics of the curves in Figs. 7a, b and Fig. 8 matches qualitatively. The above agreement is encouraging.

The above comparison would confirm that the 2D axisymmetric quasi-static finite element model established in this paper possesses a qualitative analysis reference.

Figure 9 shows the axial, hoop, radial and shear stress distributions on the wafer surface. It is found from Eq. 21 that the von Mises stress is an effective stress, whose factor includes the above four stress components. Since a 0.069 MPa down pressure is applied on the top surface of the carrier along axial direction, it induces that the axial stress has a negative value. Besides, by comparing these four stress components on wafer centre and the maximum for each stress on wafer surface listed in Table 2, it is found that the magnitude of axial stress is significantly higher than that of the other three components and its value is at least approximately ten times higher than other three stresses. Therefore, it is obvious that the main contribution to the calculated von Mises stress is the axial stress, i.e., the magnitude and profile of the von Mises stress correlate well with the axial stress component.

Figure 10 shows the axial, hoop, radial and shear strain distributions on the wafer surface. Since the axial-direction pressure is applied on the top surface of the carrier, and the four strain components on wafer centre and the maximum for each strain on wafer surface are calculated and listed in Table 3, it is found that the magnitude of axial strain is much higher than that of the other three components. Therefore, it is clear that the deformation of wafer correlates primarily with the magnitude of the axial strain.

6 Conclusions

From the simulation and analysis of the CMP model developed in this paper, the conclusions can be drawn:

1. A 2D axisymmetric quasi-static model for CMP is derived.
2. A 2D axisymmetric finite element model for CMP composed of four-layer structures of wafer carrier, carrier film, wafer and pad is developed.
3. The calculated von Mises stress distributions on the wafer surface are almost uniform, then increase gradually with a small amount. However, near the wafer edge, it would decrease in a large range. Finally, it would increase dramatically and peak significantly at the edge.
4. Due to the axial down pressure applied on the top surface of the carrier, it induces that the axial stress and strain are the primary factors that affect the von Mises stress distributions and deformation on the wafer surface.

Acknowledgements It is gratefully acknowledged that the National Science Council of the Republic of China provided funds (Grant No.: NSC 90-2212-E-237-001) for the financial support of this work.

References

1. Runnels SR, Renteln P (1993) Modeling the effect of polish pad deformation on wafer surface stress distributions during chemical-mechanical polishing. *Dielectric Sci Technol* 6:110–121
2. S. R. Runnels SR, Eyman LM (1994) Tribology analysis of chemical-mechanical polishing. *J Electrochem Soc* 141(6):1698–1701
3. Kaanta CW, Landis HS (1991) Radial uniformity control of semiconductor wafer polishing. US Patent 5,036,630, 1991
4. Wang D, Lee J, Holland K, Bibby T, Beaudoin S, Cale T (1997) Von Mises stress in chemical-mechanical polishing processes. *J Electrochem Soc* 144(3):1122–1127
5. Srinivasa-Murthy C, Wang D, Beaudoin SP, Bibby T, Holland K, Cale TS (1997) Stress distribution in chemical-mechanical polishing. *Thin Sol Film* 308:533–537
6. Baker AR (1997) The origin of the edge effects in CMP. In: *Proceedings of the Electrochemical Society* 96(22):228–237
7. Yu TK (1995) Modeling of the chemical-mechanical polishing process. In: *Proceedings of the Materials Research Society, ULSI-X Conferences*, pp 187–194
8. Tseng WT (1998) Machine-related wafer pressure distribution and its influence on chemical-mechanical polishing process. In: *The Electrochemical Society Proceedings*, pp 457
9. Castillo-Mejia D, Perlov A, Beaudoin S (2000) Qualitative prediction of SiO₂ removal rates during chemical mechanical polishing. *J Electrochem Soc* 147(12):4671–4675
10. Ahmadi G, Xia X (2001) A model for mechanical wear and abrasive particle adhesion during the chemical-mechanical polishing process. *J Electrochem Soc* 148(3):G99–G109
11. Yu TK, Yu CC, Orłowski M (1993) A statistical polishing pad model for chemical-mechanical polishing. *IEDM Tech Dig* pp 865–868
12. Rao SS (1989) *The finite element method in engineering*. Pergamon, New York